STAR FORMATION HISTORIES OF $Z \sim 1$ GALAXIES IN LEGA-C

PRISCILLA CHAUKE,[1] ARJEN VAN DER WEL,[2,1] CAMILLA PACIFICI,[3] RACHEL BEZANSON,[4] PO-FENG WU,[1] ANNA GALLAZZI,[5] KAI NOESKE,[6] CAROLINE STRAATMAN,[2] JUAN-CARLOS MUÑOS-MATEOS,[7] MARIJN FRANX,[8] IVANA BARIŠIĆ,[9] ERIC F. BELL,[10] GABRIEL B. BRAMMER,[3] JOAO CALHAU,[11] JOSHA VAN HOUDT,[9] IVO LABBÉ,[8] MICHAEL V. MASEDA,[8] ADAM MUZZIN,[12] HANS-WALTER RIX,[9] AND DAVID SOBRAL[8,11]

[1] *Max-Planck-Institut für Astronomie, Königstuhl 17, D-69117 Heidelberg, Germany*
[2] *Sterrenkundig Observatorium, Universiteit Gent, Krijgslaan 281 S9, B-9000 Gent, Belgium*
[3] *Space Telescope Science Institute, 3700 San Martin Drive, Baltimore, MD 21218, USA*
[4] *University of Pittsburgh, Department of Physics and Astronomy, 100 Allen Hall, 3941 O'Hara St, Pittsburgh PA 15260, USA*
[5] *INAF-Osservatorio Astrofisico di Arcetri, Largo Enrico, Fermi 5, I-50125 Firenze, Italy*
[6] *Experimenta Heilbronn, Kranenstraße 14, 74072, Heilbronn, Germany*
[7] *European Southern Observatory, Alonso de Cordova 3107, Casilla 19001, Vitacura, Santiago, Chile*
[8] *Leiden Observatory, Leiden University, PO Box 9513, 2300 RA Leiden, The Netherlands*
[9] *Max-Planck Institut für Astronomie, Königstuhl 17, D-69117, Heidelberg, Germany*
[10] *Department of Astronomy, University of Michigan, 1085 S. University Ave., Ann Arbor, MI 48109, USA*
[11] *Physics Department, Lancaster University, Lancaster LA1 4YB, UK*
[12] *Department of Physics and Astronomy, York University, 4700 Keele St., Toronto, Ontario, MJ3 1P3, Canada*

Submitted to ApJ

ABSTRACT

Using high resolution spectra from the VLT LEGA-C program, we reconstruct the star formation histories (SFHs) of 607 galaxies at redshifts $z = 0.6 - 1.0$ and stellar masses $\gtrsim 10^{10}\,M_\odot$ using a custom full spectrum fitting algorithm that incorporates the *emcee* and *FSPS* packages. We show that the mass-weighted age of a galaxy correlates strongly with stellar velocity dispersion (σ_*) and ongoing star-formation (SF) activity, with the stellar content in higher-σ_* galaxies having formed earlier and faster. The SFHs of quiescent galaxies are generally consistent with passive evolution since their main SF epoch, but a minority show clear evidence of a rejuvenation event in their recent past. The mean age of stars in galaxies that are star-forming is generally significantly younger, with SF peaking after $z < 1.5$ for almost all star-forming galaxies in the sample: many of these still have either constant or rising SFRs on timescales $> 100\,\mathrm{Myrs}$. This indicates that $z > 2$ progenitors of $z \sim 1$ star-forming galaxies are generally far less massive. Finally, despite considerable variance in the individual SFHs, we show that the current SF activity of massive galaxies ($> L_*$) at $z \sim 1$ correlates with SF levels at least $3\,\mathrm{Gyrs}$ prior: SFHs retain 'memory' on a large fraction of the Hubble time. Our results illustrate a novel approach to resolve the formation phase of galaxies, and in identifying their individual evolutionary paths, connects progenitors and descendants across cosmic time. This is uniquely enabled by the high-quality continuum spectroscopy provided by the LEGA-C survey.

Keywords: galaxies: star formation histories — galaxies: high-redshift — galaxies: evolution

1. INTRODUCTION

The ability to reconstruct the star-formation histories of galaxies, by characterising their stellar populations, allows one to trace their individual evolution through

chauke@mpia-hd.mpg.de

time, and thereby directly connect their descendants to their progenitors at higher redshifts. Thus far, high-redshift galaxy surveys have produced snapshots of the galaxy population at different points in cosmic time, which produces tight boundary conditions for galaxy formation models. However, the importance of the many physical processes included in these models are not directly constrained. We still do not know individual star-

formation histories (SFHs) and how these are related to global galaxy properties. To constrain galaxy formation theories more directly, 'archaeological' reconstruction can be used to trace the evolution of individual galaxies over time, and then the dependance of individual SFHs on stellar mass, stellar velocity dispersion and star-formation (SF) activity can be explored.

Reconstructing SFHs requires high resolution spectra of galaxies. Ideally, individual stars would be resolved, as they are for local dwarf galaxies (e.g., Weisz et al. 2011). However, in most cases we have to rely on integrated stellar light, though if a galaxy's main star formation (SF) epoch lies at $z > 1$, we cannot temporally resolve its stellar age distribution, even with the highest-quality spectra. While there is a plethora of high resolution spectra of galaxies in the local universe, most of these galaxies are too old (> 5 Gyrs, Gallazzi et al. 2005) to resolve their star-formation histories (SFHs) due to the similarity of stellar spectra in the age range > 5 Gyrs. The general insight gained from the 'archaeological' studies of these galaxies is that low-mass galaxies have more extended SFHs that peak at later cosmic times compared to high-mass galaxies ('downsizing', e.g., Gallazzi et al. 2005; Thomas et al. 2005, 2010). Many of these studies involved the use of fossil record methods on SDSS (Sloan Digital Sky Survey, York et al. 2000) spectra of local galaxies (e.g. Juneau et al. 2005; Thomas et al. 2005; Cid Fernandes et al. 2007; Tojeiro et al. 2009; McDermid et al. 2015; Ibarra-Medel et al. 2016). However, downsizing has also been seen in other studies, such as studies by Cimatti et al. (2006), who corrected luminosity function data of early-type galaxies by adopting the empirical luminosity dimming rate derived from the evolution of the Fundamental Plane of field and cluster massive early-type galaxies, as well as Leitner (2012), who derived the average growth of stellar mass in local star-forming galaxies using a Main Sequence Integration approach.

One approach to probe the high-redshift regime, is to obtain an integrated view of galaxy evolution. Thus far, this has been the focus of spectroscopic observations of distant galaxies: the evolution of the star-formation rate density (SFRD) in the universe has been extensively studied (e.g., Karim et al. 2011; Madau & Dickinson 2014; Khostovan et al. 2015; Abramson et al. 2016). The majority of these studies indicate that the SFRD increased from high redshift to $z \sim 2$, and has since been decreasing steeply. Coupled with this, are number density evolution studies which show an increasingly dominant population of quiescent galaxies (e.g., Pozzetti et al. 2010; Brammer et al. 2011; Moustakas et al. 2013; Muzzin et al. 2013a).

Another approach is to use photometric measurements to trace SFHs, however, individual galaxy evolution is not easily traced with this method due to high uncertainties. In this case, one can investigate average SFHs of galaxies as Pacifici et al. (2016) have done by applying spectral energy distribution models to compute the median SFHs of 845 quiescent galaxies at $0.2 < z < 2.1$. They found that galaxy stellar mass is a driving factor in determining how evolved galaxies are, with high mass galaxies being the most evolved at any time. The limitation with these approaches is that we cannot connect progenitors to descendants: studies from mass-matched samples have resulted in multiple solutions (e.g., Torrey et al. 2017). To understand the mechanics of how galaxies evolve, it is crucial to expand our view from focusing on the population of galaxies as a whole, to investigating how the star-formation rate (SFR) of individual galaxies varies with time.

Probing the SFHs of individual galaxies, however, still requires high-resolution, high-quality stellar continuum spectra, which are expensive to obtain. Consequently, high-redshift samples are small and often selected with criteria to optimize data quality and sample size rather than represent the full galaxy population. Jørgensen & Chiboucas (2013) obtained spectra for ~ 80 cluster galaxies at $z = 0.5 - 0.9$ and found ages of $3 - 6$ Gyrs, consistent with passive evolution between $z \sim 2$ and the present. Stellar population measurements of ~ 70 $z \sim 0.7$ galaxies with stellar masses $> 10^{10}$ $M_\odot$ were performed by Gallazzi et al. (2014); they found that passive galaxies have ages and metallicities consistent with those of present-day galaxies, and that star-forming galaxies require further star-formation and metal enrichment to evolve into present-day descendants. Choi et al. (2014) analysed stacked spectra of thousands of passive galaxies in the redshift range $0.1 < z < 0.7$ and also found age evolution consistent with mostly passive evolution, with little dependence on mass at $z > 0.5$. Belli et al. (2015) measured ages of $1 - 4$ Gyrs for several dozen passive galaxies at redshifts $1 < z < 1.6$, indicating that we are approaching the cosmic epoch at which massive, passive galaxies stopped forming stars. Finally, at $z > 1.5$, measurements are limited to stacked spectra (e.g., Whitaker et al. 2013; Onodera et al. 2015) or sample sizes ranging from single objects to a handful (e.g., van Dokkum & Brammer 2010; Toft et al. 2012; van de Sande et al. 2013; Kriek et al. 2016). The typical age of massive, passive galaxies at those redshifts is found to be 1 Gyr or less, with short formation time scales. From this brief review, it is evident that samples at large lookback time are generally small and/or stacked. Furthermore, ages are usually estimated by assuming a single stellar popu-

lation, which is arguably justified for very massive galaxies at late cosmic epochs, but not in general.

The LEGA-C (Large Early Galaxy Astrophysics Census, van der Wel et al. 2016) survey is collecting high S/N spectra of ~ 3000 galaxies in the redshift range $0.6 < z < 1$, selected only by their K-band magnitude (a proxy for stellar mass). The data, which are comparable in quality to those obtained in the nearby universe, probe the internal kinematics of stars and gas, and the ages and metallicities of stellar populations. This enables us, for the first time, to reconstruct the SFHs of individual galaxies at large look-back time that are representative of the population. These reconstructed SFHs can provide a direct connection between progenitors and descendants, and allow us to constrain when, and how quickly, galaxies formed their stars.

Over the past decade, there have been several algorithms developed to recover SFHs, viz. *MOPED*, *STARLIGHT*, *STECMAP*, *VESPA*, *ULYSS* and *FIRE-FLY* (Heavens et al. 2000; Cid Fernandes et al. 2005; Ocvirk et al. 2006; Tojeiro et al. 2007; Koleva et al. 2009; Wilkinson et al. 2015). We develop our own approach in this study to tailor the problem for galaxies at $z \sim 1$. The main differences between our algorithm and some of those listed above are the use of composite stellar populations (a group of stars which range in age within a given interval) instead of simple stellar populations (stars born from a single burst in star formation); using a defined set of template spectra which allow for direct comparisons of the SFHs; as well as the assumption of constant star formation within a given time interval. The galaxy spectra are also not continuum-normalised in the fitting process, but photometry is used to calibrate the fluxes.

The goal of this paper is to reconstruct the SFHs of galaxies in the LEGA-C sample and investigate the dependance of individual SFHs on stellar mass, stellar velocity dispersion and star-formation (SF) activity. The paper is outlined as follows. In Section 2 we give a brief overview of the LEGA-C dataset. In Section 3 we introduce the model for reconstructing the SFHs of the galaxies as well as tests of the model. In Section 4 we present a sample of the resultant fits and general trends of measured parameters. In Section 5 we investigate the SFH as a function of stellar velocity dispersion and stellar mass. We demonstrate that we can verify the relation between the evolution of SFHs and mass, and we investigate the variation in the reconstructed SFHs, at fixed stellar velocity dispersion. Finally, in Section 5 we summarise the results. A ΛCDM model is assumed with $H_0 = 67.7 \, \mathrm{km \, s^{-1} \, Mpc^{-1}}$, $\Omega_m = 0.3$ and $\Omega_\Lambda = 0.7$.

2. DATA

LEGA-C (van der Wel et al. 2016) is an ongoing ESO Public Spectroscopic survey with VLT/VIMOS of ~ 3000 galaxies in the COSMOS field ($R.A. = 10^h00^m$; $Dec. = +2°12'$). The galaxies were selected from the Ultra-VISTA catalog (Muzzin et al. 2013b), with redshifts in the range $0.6 < z < 1.0$. The galaxies were K-band selected with a magnitude limit ranging from $K(AB) = 21.08$ at z = 0.6 to $K(AB) = 20.7$ at z = 0.8 to $K(AB) = 20.36$ at z = 1.0 (stellar masses $M_* > 10^{10} \, \mathrm{M_\odot}$). These criteria were chosen to reduce the dependence on variations in age, SF activity and extinction, as well as ensure that the targets were bright enough in the observed wavelength range ($0.6\mu m - 0.9\mu m$) to obtain high quality, high resolution spectra (R ~ 3000). Each galaxy is observed for $\sim 20 \, \mathrm{h}$, which results in spectra with $S/N \sim 20 \, \mathrm{\mathring{A}^{-1}}$.

The analyses in this work are based on the first-year data release[1], which contains spectra of 892 galaxies, 678 of which are in the primary sample and have a $S/N > 5 \, \mathrm{\mathring{A}^{-1}}$ between rest-frame wavelengths $4000 \, \mathrm{\mathring{A}}$ and $4300 \, \mathrm{\mathring{A}}$ (typically, $S/N \sim 20 \, \mathrm{\mathring{A}^{-1}}$). Emission line subtracted spectra are used in the fitting algorithm; therefore, the emission line spectrum of each galaxy, computed using the Penalized Pixel-Fitting method (pPXF, Cappellari & Emsellem 2004), is subtracted from the observed spectrum. For details of the emission line fitting procedure, see Bezanson et al. (2018, submitted to ApJ). As part of the analysis of the model, we use the following measured quantities: stellar velocity dispersions (σ_*), 4000 Å break (D_n4000) and Hδ equivalent width indices [EW(Hδ)], U-V colours, stellar masses ($M_{*,FAST}$), UV+IR SFRs, and UV+IR specific SFRs (sSFR$_{UV+IR}$). Stellar masses are determined using FAST (Kriek et al. 2009) based on photometric measurements, Bruzual & Charlot (2003) stellar population libraries, adopting a Chabrier (2003) Initial Mass Function (IMF), Calzetti et al. (2000) dust extinction, and exponentially declining SFRs. The UV+IR SFRs are estimated from the UV and IR luminosities, following Whitaker et al. (2012). For details of the data reduction procedure, see van der Wel et al. (2016).

3. SPECTRAL FITTING TECHNIQUE

3.1. *Stellar Population Model*

To reconstruct the SFHs of galaxies, one needs to gauge the various ages of stellar populations within these galaxies. This is done using stellar population spectra generated with the Python implementation of the Flex-

---

[1] http://www.eso.org/qi/catalogQuery/index/93

Table 1. Properties of the *FSPS* template spectra.

Age Bin[a]	SFR[b]	M_*[c]	L_{bol}[d]
log(yr)	$M_\odot$/yr	$M_\odot$	$\log(L_\odot)$
$0.000 - 8.000$	1.000×10^{-8}	0.837	1.964
$8.000 - 8.300$	1.005×10^{-8}	0.711	0.885
$8.300 - 8.475$	1.010×10^{-8}	0.748	0.650
$8.475 - 8.650$	6.750×10^{-9}	0.731	0.497
$8.650 - 8.750$	8.646×10^{-9}	0.718	0.382
$8.750 - 8.875$	5.332×10^{-9}	0.707	0.285
$8.875 - 9.000$	3.998×10^{-9}	0.695	0.187
$9.000 - 9.075$	5.305×10^{-9}	0.685	0.127
$9.075 - 9.225$	2.040×10^{-9}	0.671	0.099
$9.225 - 9.375$	1.444×10^{-9}	0.652	-0.043
$9.375 - 9.525$	1.022×10^{-9}	0.639	-0.161
$9.525 - 9.845$	2.681×10^{-10}	0.618	-0.347

[a] Age interval of CSP templates.

[b] SFR s.t. $1\,M_\odot$ of stars formed within the interval.

[c] Stellar mass (including stellar remnants) with mass loss accounted for.
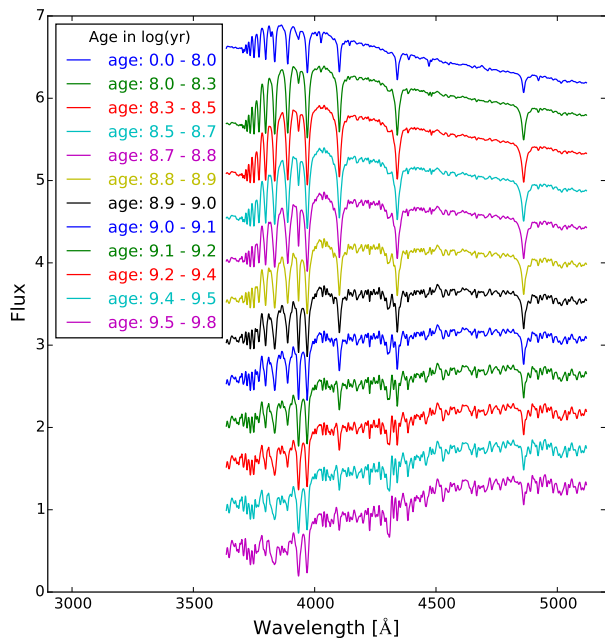
[d] Bolometric luminosity.

Figure 1. Template CSP spectra used to fit LEGA-C galaxies. They were generated from *FSPS*, using the time intervals listed in Table 1, with solar metallicity and arbitrary velocity dispersion; and they have been normalised and shifted here for comparison purposes.

ible Stellar Population Synthesis package (*FSPS v3.0*; Conroy & Gunn 2010; Conroy et al. 2009; Foreman-Mackey et al. 2014), using the MILES spectral library (Sánchez-Blázquez et al. 2006), Padova isochrones (Girardi et al. 2000; Marigo & Girardi 2007; Marigo et al. 2008) and a Kroupa initial mass function (Kroupa et al. 2001).

A galaxy spectrum is approximated to be a linear combination of template spectra at varying ages, attenuated by dust:

$$f_\lambda = \sum_{i=1}^{n} m_i T_{\lambda,i} 10^{-0.4 k_\lambda E(B-V)_i}, \qquad (1)$$

$$k_\lambda = 2.659\Big(-2.156 + \frac{1.509}{\lambda} - \frac{0.198}{\lambda^2} + \frac{0.011}{\lambda^3}\Big) + 4.05$$

where n is the number of stellar population spectra to fit to the galaxy, $T_{\lambda,i}$ are the template spectra, m_i are the weights that scale the templates to match the spectra of the galaxy, k_λ is the reddening curve (Calzetti et al. 2000), and $E(B-V)_i$ are the dust reddening values.

We generate 12 composite stellar population spectra (CSPs), with solar metallicity (see Section 3.3), covering ages from 0 to about 7 Gyrs, the age of the Universe in LEGA-C's redshift range. To determine the intervals of the 12 age bins of the CSPs, simple stellar population spectra (SSPs) were generated and the cumulative absolute difference from one spectrum to another was calculated as the age was increased; which was then divided into 12 percentiles with equal width (see Table 1 and Figure 1 for the properties of the CSPs in each age bin). This method of determining the time intervals generates template spectra that optimise the temporal sampling of an evolving stellar population. In practice, the age bins are ~ 0.15 dex wide over the age range $0 - 7$ Gyrs.

The template spectra are generated with a constant SFR and are normalised such that $1\,M_\odot$ of stars are formed within each time bin (stellar masses include stellar remnants). Note that there is mass loss in each bin as massive stars die off (see Table 1). We assume a constant SFR within each time bin as it presents a more realistic evolution of a galaxy's star formation with time, and can take into account rapid changes in the SFH. Choosing SSP templates would not lead to significantly different SFHs, however, it would lead to aliasing effects when reconstructing the SFHs for samples of galaxies. The templates are also broadened to the velocity dispersion of the galaxies (Bezanson et al. 2018, submitted to ApJ). It is assumed that dust reddening is the same for all populations except for the youngest population (age < 100 Myrs). Dust extinction is expected to be different for young stellar populations as they are usually observed to be nested in the dust of their molecular birth
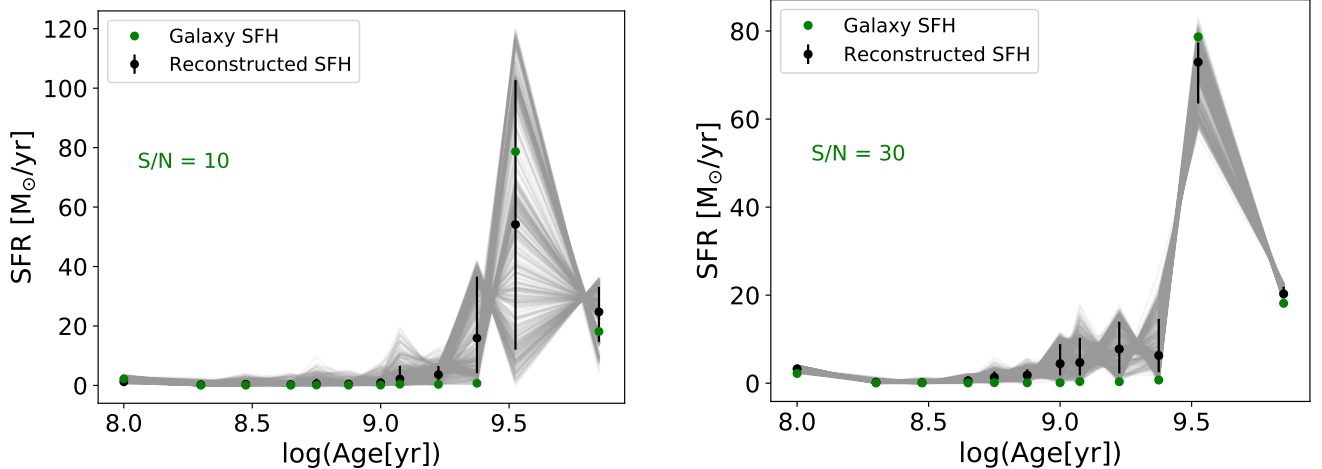
Figure 2. Reconstructed SFH (black) of a synthetic galaxy (green) with S/N $= 10\,\text{\AA}^{-1}$ (left) and S/N $= 30\,\text{\AA}^{-1}$ (right). The converged walkers are shown in grey and the upper and lower uncertainties are based on the 16th and 84th percentiles, respectively, as explained in Section 3.2. By S/N $= 30\,\text{\AA}^{-1}$, the recovered SFHs predict the stellar mass, age and luminosity with precision $\leq 0.1\,\text{dex}$.

clouds (Charlot & Fall 2000). Therefore, two dust reddening values are fit for: $E(B-V)_1$, for the age range $0 - 100\,\text{Myrs}$, and $E(B-V)_2$, for the rest of the age ranges.

3.2. Fitting Algorithm

To find the optimal values for the 14 parameters, viz. the 12 weight factors (m_i) for the 12 CSP templates and 2 dust reddening values $(E(B-V)_i)$, we used *emcee*, a Python implementation of an affine invariant ensemble sampler for MCMC (Foreman-Mackey et al. 2013) which was proposed by Goodman & Weare (2010). It uses MCMC 'walkers' which randomly explore the parameter space, where each proposed step for a given walker depends on the positions of all the other walkers in the ensemble, with the aim of converging to the most likely parameter values.

The priors for the 14 parameters were set such that all parameter values were always greater or equal to 0, and the upper limit for $E(B-V)_i$ was set to 3. The parameter value for the youngest bin was initially set to be equal to the measured SFR from UV+IR measurements, but it was allowed to vary between 1/3 and 3 times that value during the fitting process, allowing for measurement errors. For the other bins, the best fitting single template, computed using least-squares fitting, was assigned all the stellar mass, with all other parameter values set to 10^{-6}. Starting with equal SFRs in all bins also recovers the SFHs, however, the algorithm may take longer to converge to the optimal values.

For each galaxy, 100 MCMC walkers were used, initiated in a small region around the starting values mentioned above. A total of 20000 samples were taken and 1000 steps were kept after burn-in. The mean acceptance fraction was $\gtrsim 0.2$ and the typical autocorrelation time was ~ 95 iterations. The optimal values for the parameters are taken as the 50th percentile of the list of samples of the converged walkers, and the lower and upper uncertainties are the 16th and 84th percentiles, respectively. The fitting algorithm resulted in 607 good fits based on their normalised χ^2 values (< 5, from visual inspection of the fits), and these were used in the analyses. The spectra that were not well-fit were mainly due to low S/N and AGN.

3.3. Robustness of Fitting Results

To assess the robustness of the model, we performed the following tests: generate and fit synthetic spectra; compare model stellar mass measurements of the LEGA-C population with those obtained from broad-band photometry (see Section 2); fit a sample of SDSS spectra and compare model stellar masses with literature measurements; and test the assumption of solar metallicity.

Synthetic galaxy spectra were generated with varying SFHs using the CSPs in Section 3.1, including simulated noise that mimics LEGA-C variance spectra, to compare how well the algorithm recovered the SFHs. 20 SFHs were generated for each S/N (5, 10, 20, 30, 40, 50 and $60\,\text{\AA}^{-1}$), and the average deviations of the true $a_{<MW>}$, stellar mass and luminosity from the best-fitting model parameters were computed. In general,

the model sufficiently recovered the SFHs, however, we note that the quality of the results depends on the noise introduced into a spectrum (see Figure 2 for two examples). Stellar mass and luminosity are recovered with precision ≤ 0.1 dex for S/N≥ 20, while $a_{<MW>}$ only requires S/N≥ 10 to reach the same level of precision. We note that these tests only constrain the purely random uncertainties due to the noise in the spectra while they do not include systematic errors in the data (e.g., sky subtraction, flux calibration) and systematic uncertainties in the FSPS model spectra.

Imposing the MCMC model on the LEGA-C dataset and comparing the stellar masses measured from the model to those measured from FAST (using photometric measurements), resulted in very good agreement between the two methods, with a scatter of ~ 0.2 dex and an offset of ~ 0.03 dex. This scatter is larger than the formal uncertainty on our mass measurements (~ 0.15 dex).

We used the fitting algorithm on a sample of 20 SDSS spectra of massive local galaxies ($z \sim 0.1$), selected by stellar mass ($M_* > 10^{10}$), to determine whether the model could recover the stellar masses measured in the literature. We compared the model stellar masses to measurements from the Portsmouth method (Maraston et al. 2009) and found satisfactory agreement, with a ~ 0.2 dex scatter. The maximum age of the templates was increased to ~ 12 Gyrs to account for the low redshift (~ 0.1) of the SDSS galaxies. The 0.2 dex random uncertainty is an indication of how results vary as a consequence of using a different SPS model (here, Maraston et al. (2009) vs. FSPS) and fitting algorithm.

Solar metallicity was used to generate all the CSPs because according to Gallazzi et al. (2005, 2014), the metallicity-mass relation flattens out to solar metallicity in LEGA-C's mass range ($\log(M) \gtrsim 10.5$), for $z \sim 0.7$ galaxies. On the other hand, Jørgensen et al. (2017) find evidence for evolution in the metallicity for cluster galaxies, as well as a trend of increasing metallicity with increasing velocity dispersion. We test our approach by repeating our fits with implausibly low metallicity ($0.4 \, Z_\odot$, sub-solar) and high metallicity ($2.5 \, Z_\odot$, super-solar) CSPs. We find no significant differences in the χ^2 values of the fits, but, naturally, the inferred ages depend on the chosen metallicity. If we assign sub-solar metallicity for galaxies in our sample, the derived mass-weighted and light-weighted ages are older by 0.05 and 0.08 dex, respectively, with a standard deviation of 0.16 and 0.24 dex, respectively. If we assign super-solar metallicity for the sample, the light-weighted ages are younger by 0.03 dex, with a standard deviation of 0.20 dex. The mass-weighted age changes from solar to

high metallicity are not normally distributed: 80% of the galaxies have the same age to within 0.20 dex, while for the remaining 20% the change in age ranges from 0.2 to 0.9 dex. However, only 10 of these galaxies' mass-weighted ages change by ≥ 0.5 dex and they have a mean light-weighted age of ~ 0.4 Gyr. The age changes do not depend on the measured stellar mass or stellar velocity dispersion.

The velocity dispersion-metallicity trend presented by Jørgensen et al. (2017) implies that our assumption of solar metallicity for all galaxies may introduce a correlation between velocity dispersion and age. Our tests show that across the velocity dispersion range $\sigma_* = 100-250 \, \text{km s}^{-1}$, the magnitude of this effect would be at most 0.15 dex and likely less. This potential bias is insufficient to explain the σ_*-age relation we find in Section 4.2. Follow-up studies that explore the interdependence of age, metallicity and other galaxy properties will need to take metallicity variations into account.

4. FITTING RESULTS

4.1. Model Outputs

Figure 3 shows the distribution of the model-measured stellar masses ($M_{*,FIT}$, left panel), mean mass-weighted ages[2] ($a_{<MW>}$, middle panel) and mean light-weighted ages[2] ($a_{<LW>}$, right panel) of the LEGA-C sample, along with the distribution of uncertainties for each parameter. The distributions are separated into the quiescent (red) and star-forming (blue) populations to show the differences in the distributions based on current SF activity (see Section 5). The galaxies in the LEGA-C sample span a broad range of ages: $a_{<LW>}$ can be as young as 60 Myrs and as old as 4.8 Gyrs, and has a median value of 1.2 Gyrs (see Figure 3). $a_{<MW>}$ ranges from about 400 Myrs to about 5.2 Gyrs, with a median value of 3.8 Gyrs. However, most of these galaxies are old, with about 60% being older than 3 Gyrs. The $M_{*,FIT}$ of the galaxies ranges from $\sim 2 \times 10^9 \, M_\odot$ to $\sim 4 \times 10^{11} \, M_\odot$, with a median value of about $6 \times 10^{10} \, M_\odot$. The formal age and mass uncertainties lie in the ranges 1-60% and 1-40%, respectively. As stated in Section 3.3, these uncertainties do not include systematic errors.

4.2. Sample SFHs

Figure 4 shows the spectra of a sample of LEGA-C galaxies (in $a_{<MW>}$ order) along with the best-fitting model spectra as described by Equation 1 using the optimal parameter values from *emcee*. The weight

---

[2] Mean mass-weighted and light-weighted ages are obtained by averaging the midpoint ages of the CSPs weighted by luminosity and mass, respectively.
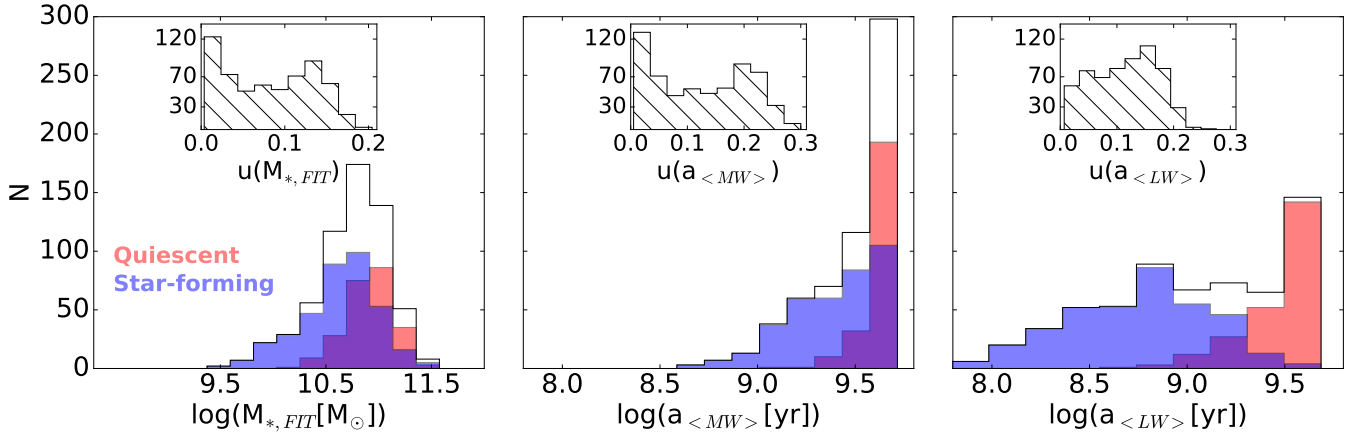
Figure 3. Distributions of $M_{*,FIT}$ (left), $a_{<MW>}$ (middle) and $a_{<LW>}$ (right) of the LEGA-C sample. The quiescent and star-forming populations (as defined in Section 5.1) are shown in red and blue, respectively. The distribution of the uncertainties for each parameter are shown at the top of each figure.

factors, m_i, represent the star formation histories of these galaxies (shown on the bottom-right of each figure). The resultant normalised χ^2, dust reddening values $(E(B-V)_i)$, stellar masses $(M_{*,FIT})$, luminosities (L_{FIT}) and mean mass-weighted ages $(a_{<MW>})$ from the model are shown in red. The sample was selected to display the wide range of SFHs recovered.

The reconstructed SFHs reveal that although most galaxies at $z \sim 1$ have $a_{<MW>} > 3\,\mathrm{Gyrs}$, the sample spans a wide range of histories. For the older massive galaxies, the oldest template (stars in the age range $\sim$3-7 Gyrs) contributes to the majority of their mass. Some of these galaxies only contain the oldest stars and have since been quiescent, i.e. for the past $\sim 3\,\mathrm{Gyrs}$ (see the SFHs of 108361, 211736 and 130052 in Figure 4). However, some galaxies were quiescent for several Gyrs and then had a renewed period of growth, either due to SF rejuvenation, or merging with a younger population. A merger could result in either an integration of the younger population with no further activity, or trigger bursts of star formation. This young population of stars accounts for $\sim 10\%$ of the mass of these galaxies (e.g. 206042, 131869 and 131393 in Figure 4). We will explore the frequency of such rejuvenation events in more detail in a follow-up study.

4.3. General Trends

Figure 5(a) presents the distribution of EW(Hδ) as a function of the D_n4000 break colour-coded by the time after which the final 10% of stars were formed (a_{10}, left

panel), $a_{<LW>}$ (middle panel) [3] and $a_{<MW>}$ (right panel), estimated from the model. The EW(Hδ)-D_n4000 distribution is analysed in depth in Wu et al. (2018). As expected, for all three age parameters, galaxies generally evolve from the upper-left region (high EW(Hδ) and low D_n4000) to the lower-right region (low EW(Hδ) and high D_n4000) as they age. a_{10} and $a_{<LW>}$ are more correlated with each other than $a_{<MW>}$ because they track young stars; they also have smoother transitions in the EW(Hδ)-D_n4000 plane because those features primarily track recent SF activity ($\lesssim 1\,\mathrm{Gyr}$). Figure 5(b) shows the rest-frame U-V colour as a function of restframe V-J colour-coded by the same 3 age parameters as above. Once again, expected trends are seen: a_{10}, $a_{<LW>}$ and $a_{<MW>}$ correlate with the restframe colours as U-V and V-J primarily reflect recent star formation ($\sim 1\,\mathrm{Gyr}$). There is a notable population of old galaxies ($a_{<MW>} > 3.5\,\mathrm{Gyrs}$) with relatively blue colours, which indicates that these galaxies have extended SFHs.

To demonstrate the validity of the old galaxies ($a_{<MW>} > 3.5\,\mathrm{Gyrs}$) in the young region of the EW(Hδ)-D_n4000 plane, i.e. galaxies in red in Figure 5's right panel, with $D_n4000 < 1.3$ and EW(Hδ) > 2, we refer to their SFHs. These galaxies formed most of their stars early on, but also have significant recent star formation. While some seem to have been quiescent at some point in their history before they were possibly rejuvenated or merged with another galaxy (e.g. 206042 in Figure 4), others formed stars throughout their history (e.g. 210003 in Figure 4). Moreover, the
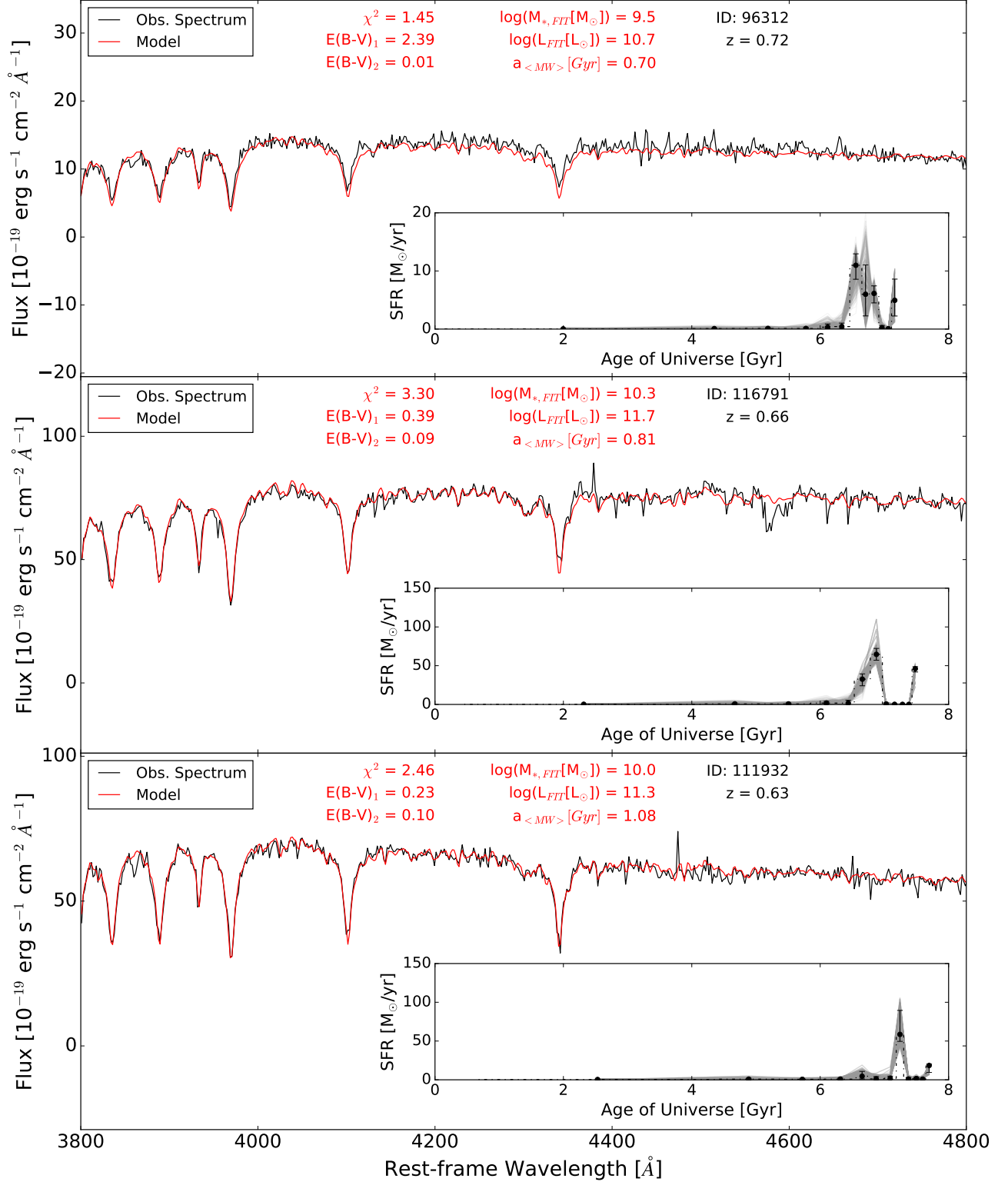
---

[3]

Figure 4. Sample of emission line subtracted spectra of 12 LEGA-C galaxies with the best fitting model obtained from combining the 12 template spectra using MCMC. The bottom-right figure, in each plot, is the reconstructed star formation history (the converged walkers are shown in grey). The MCMC resultant mass, luminosity, mass-weighted age and dust reddening values are shown in red. The spectra are ordered by $a_{<MW>}$.
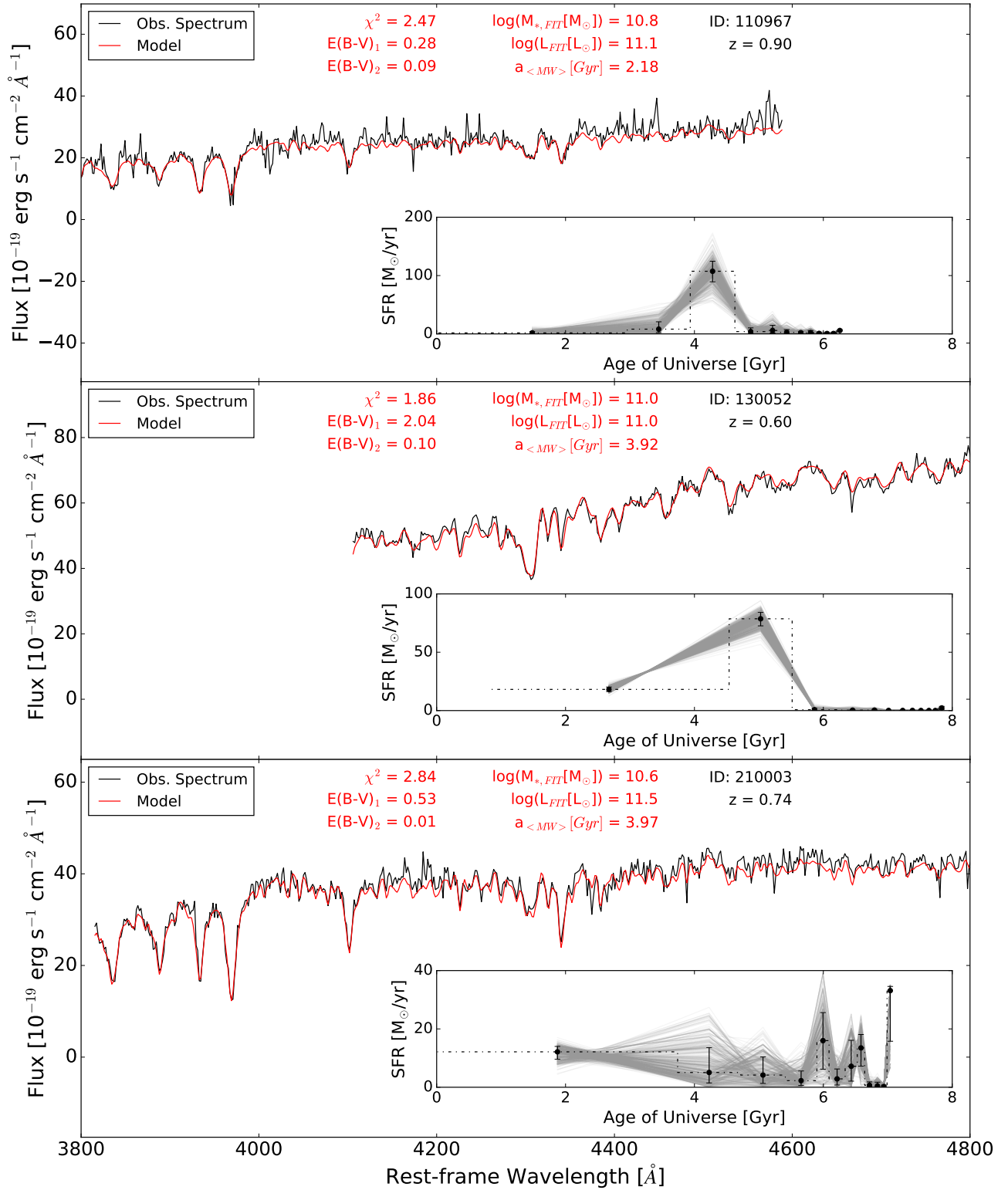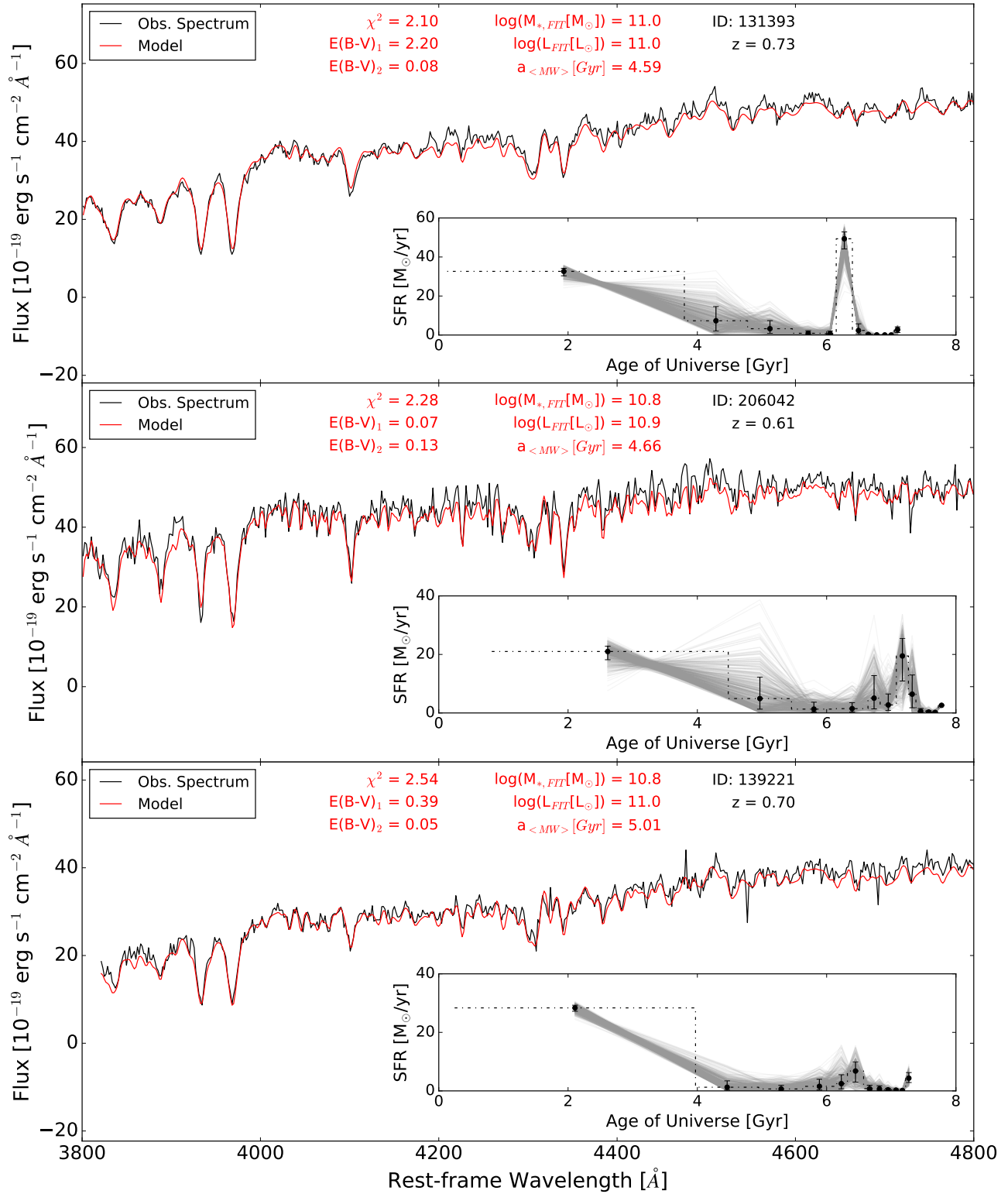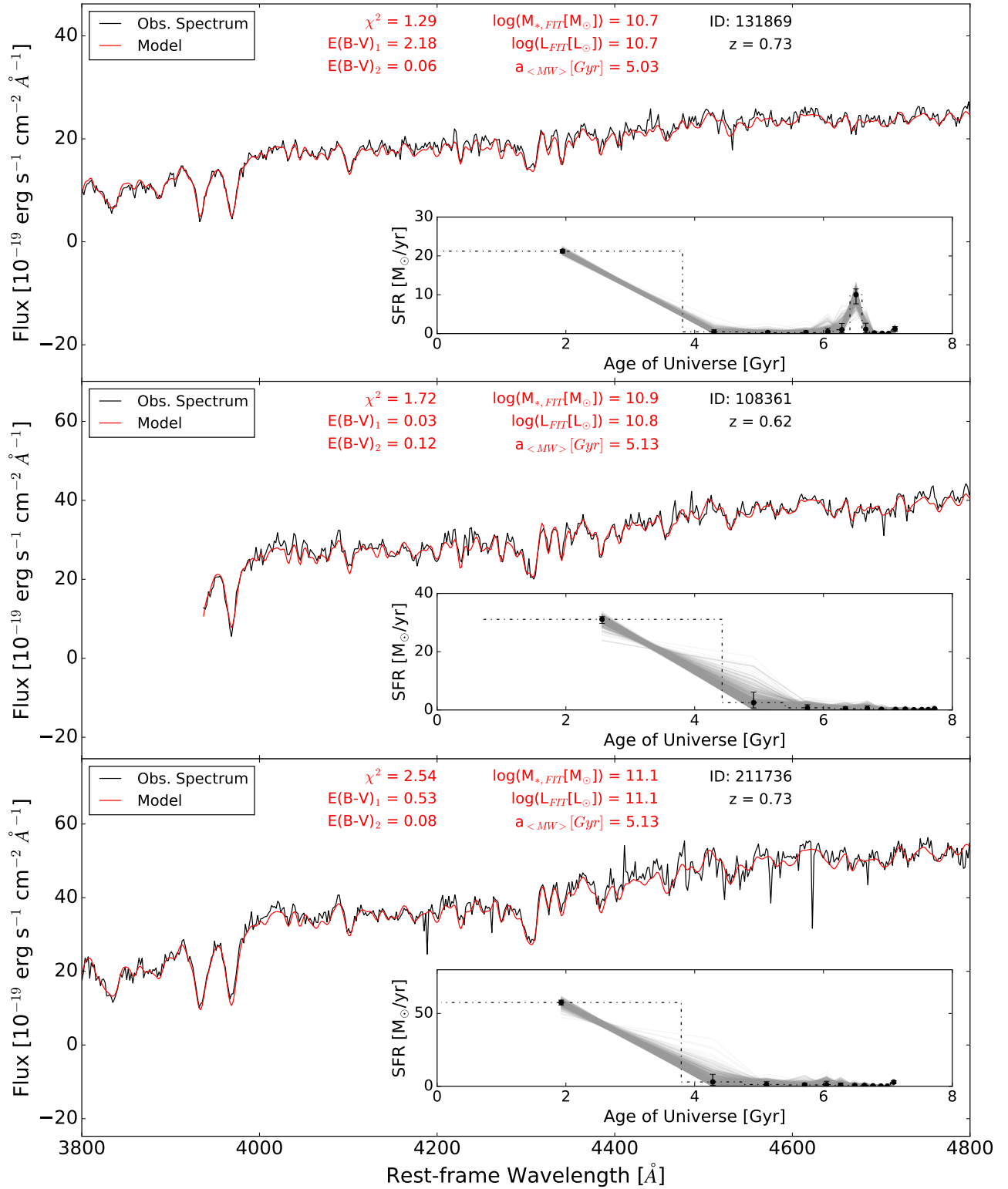
Figure 4 (Continued).
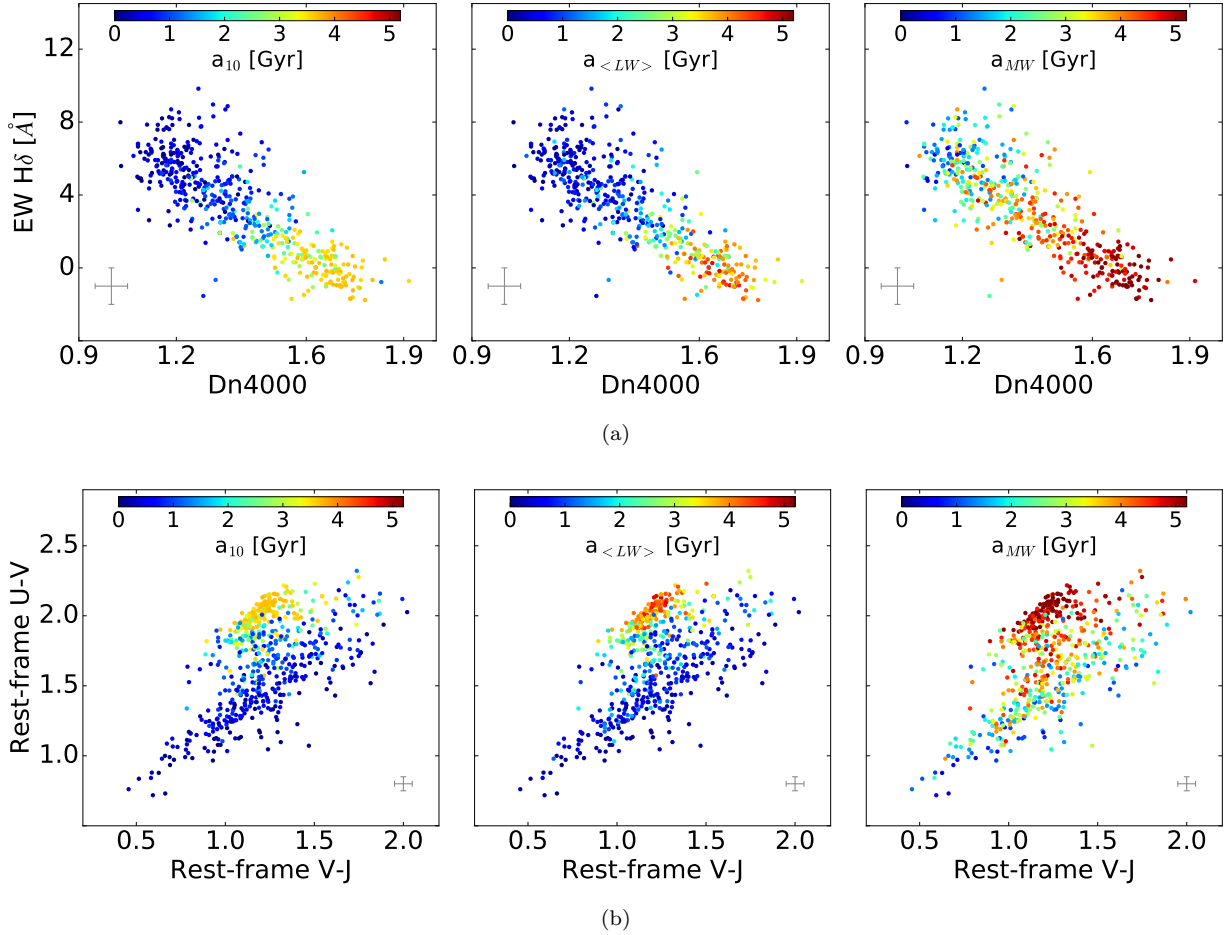
Figure 4 (Continued).

Figure 4 (Continued).

(a)

(b)

Figure 5. EW(Hδ) versus D$_n$4000 (upper panel) and U-V colour versus V-J colour (lower panel) colour-coded by the time after which the final 10% of stars were formed (left), the mean light-weighted age (middle), and the mean mass-weighted age (right). Typical error bars are indicated in grey.

presence of young and old populations can be seen in their spectra: they have clearly visible Balmer lines, characteristic of younger galaxies; but they also have H and K absorption lines of singly ionized Calcium with similar strengths, which is typical of older galaxies, in addition to the presence of the G-band (absorption lines of the CH molecule) around 4300 Å. As a test, we reran the fits of these galaxies excluding the 3 oldest templates and found that the spectra cannot be well fit.

There is also a population of galaxies that seem to contain only young stars (e.g. 111932 and 116791 in Figure 4), which would imply that these galaxies formed more than 90% of their mass recently (when the Universe was > 6 Gyrs). To test if young populations are 'outshining' the rest of these galaxies, i.e. if there are hidden populations of old stars, we reran the fits of these galaxies allowing only the oldest template parameter to vary. We found that the contribution in mass of the old population can increase by ∼ 5 − 10% before the normalised χ^2 changes by more than 0.08 dex. The change in χ^2

is mainly due to the continuum shape of the spectra. Therefore, these galaxies do not harbour significant populations of old stars that are concealed by the light of very young stars.

5. SFHS OF THE GALAXY POPULATION

5.1. *Correlations between Age, M$_{*,FIT}$ and σ$_*$*

Figure 6 shows a$_{<MW>}$ as a function of stellar mass (M$_{*,FIT}$, left panel) and stellar velocity dispersion (σ$_*$, right panel) colour-coded by current SF activity, i.e. whether the galaxy is quiescent (log(sSFR$_{UV+IR}$[Gyr^{-1}]) < −1) or star-forming. Selecting quiescent galaxies by their U-V and V-J colors would result in similar trends. a$_{<MW>}$ generally correlates more strongly with M$_{*,FIT}$ than σ$_*$. However, there is a σ$_*$ threshold above which galaxies are almost exclusively old and quiescent: galaxies with σ$_*$ > 200 − 250 km s^{-1} and a$_{<MW>}$ < 4 Gyrs are very rare. Such a clear threshold does not exist for M$_{*,FIT}$:
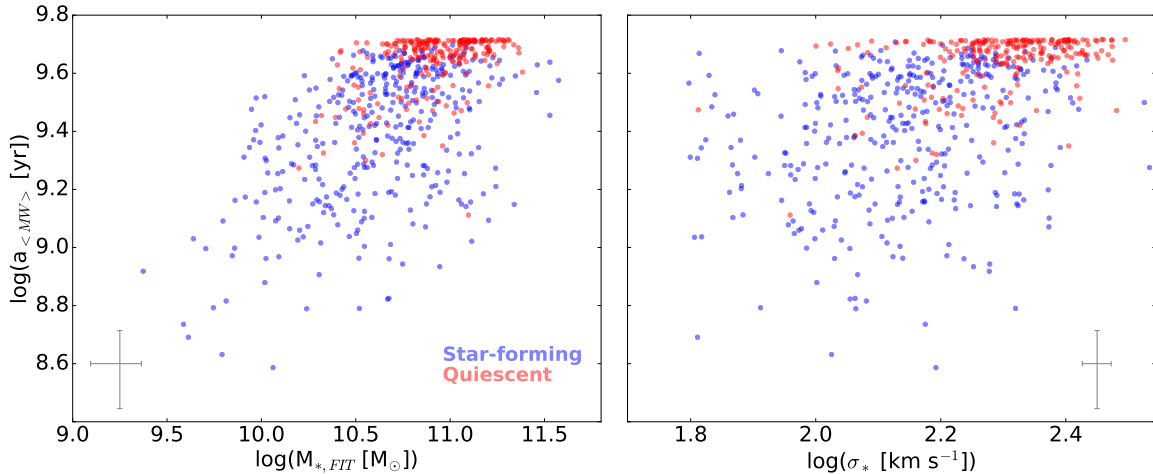
Figure 6. $a_{<MW>}$ as a function of $M_{*,FIT}$ (left) and σ_* (right). The star-forming and quiescent populations are indicated in blue and red, respectively, and typical error bars are indicated in grey. Galaxies with $\sigma_* \gtrsim 200\,\mathrm{km\,s^{-1}}$ are almost exclusively old (> 4 Gyrs) and quiescent, which indicates that σ_* is a stronger predictor of age and SF activity.

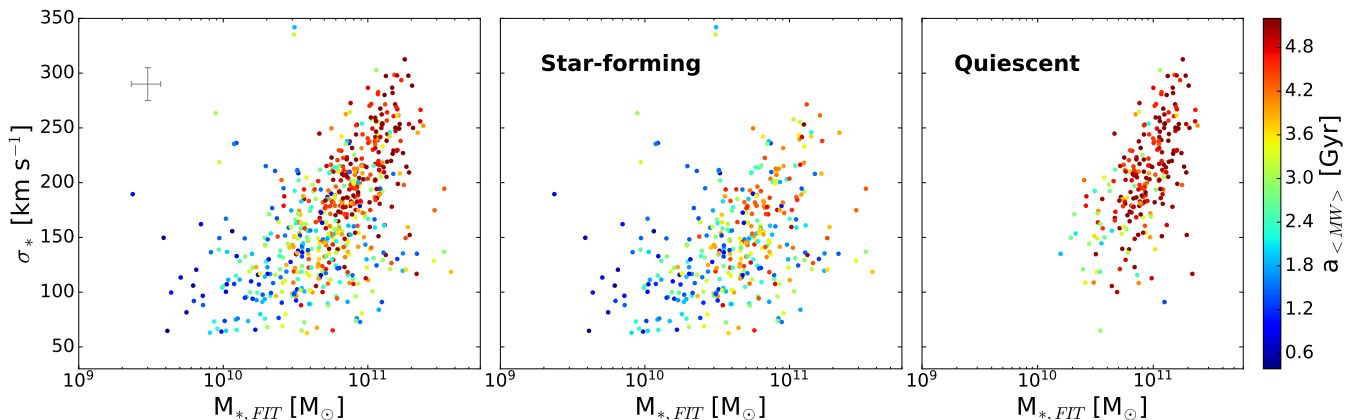**Figure 7.** σ_* versus $M_{*,FIT}$, colour-coded by $a_{<MW>}$. The star-forming and quiescent populations are shown in the middle and right panels, respectively. Typical error bars are indicated in grey. The clear separation between young and old galaxies at $\sigma_* \sim 170\,\mathrm{km\,s^{-1}}$ shows a stronger correlation between $a_{<MW>}$ and σ_* over $M_{*,FIT}$, which also depends on the current SF activity.

high-mass galaxies ($M_{*,FIT} \gtrsim 10^{11}\,M_\odot$) show a variety of ages.

To further illustrate these trends, we show σ_* as a function of $M_{*,FIT}$ colour-coded by $a_{<MW>}$ (left panel) and divided by current SF activity (middle and right panels) in Figure 7. There is a discernible separation between old (> 4 Gyrs) and young (< 4 Gyrs) galaxies at a velocity dispersion of $\sigma_* \sim 170\,\mathrm{km\,s^{-1}}$. Taken together with the trends seen in Figure 6, we can conclude that $\sigma_* > 250\,\mathrm{km\,s^{-1}}$ is a sufficient requirement for having an old age and $\sigma_* \sim 170\,\mathrm{km\,s^{-1}}$ is a necessary requirement for old age. This extends the properties of present-day

early-type galaxies, for which a correlation between velocity dispersion (and closely related quantities such as surface mass density and central mass density) and stellar age has been shown to be more fundamental than age trends with stellar mass (Kauffmann et al. 2003; van der Wel et al. 2009; Graves et al. 2009), to higher redshift. Our results also extend the widely reported correlation between velocity dispersion (as well as surface mass density and central mass density) and SF activity (e.g., Franx et al. 2008; Mosleh et al. 2017; Barro et al. 2017) to an underlying correlation with overall stellar age.
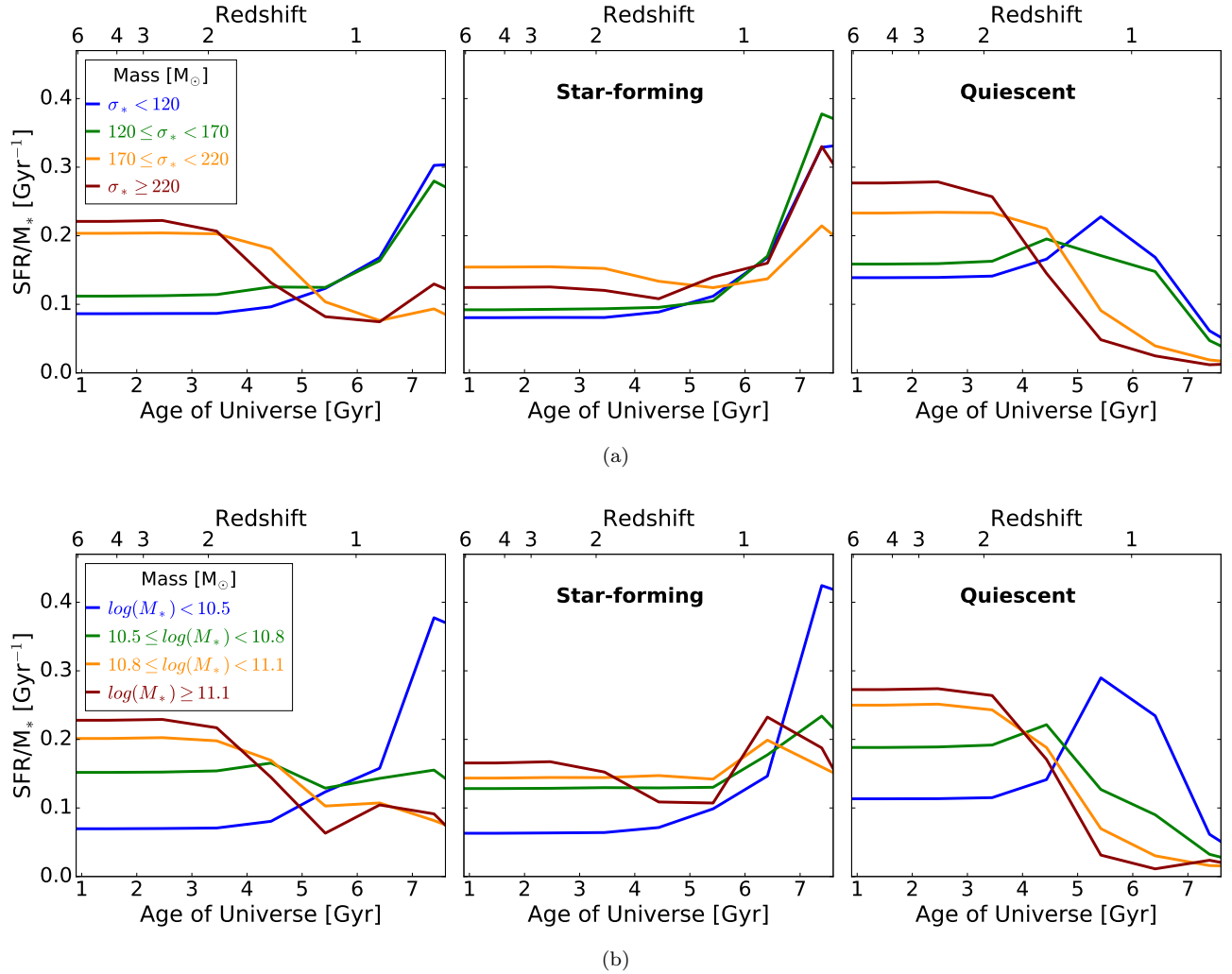
(a)

(b)

Figure 8. Ensemble-averaged SFHs of LEGA-C galaxies, normalised by stellar mass and separated into various σ_* (top) and $M_{*,FIT}$, bins (bottom). The histories are divided into the star-forming and quiescent populations in the middle and right panels, respectively. The stellar content in massive galaxies formed earlier and faster, regardless of current SF activity.

The scaling relation between σ_* and black hole (BH) mass implies that large BH mass is correlated with early SF and the ceasing thereof. Such a scenario is supported by the direct correlation between BH mass and SF activity (e.g., Terrazas et al. 2016) and the large fraction of radio AGN among galaxies with large velocity dispersions both at low and high redshift (e.g., Best et al. 2005; Barišić et al. 2017).

It is interesting to note that the correlation between $a_{<MW>}$ and σ_* seen in Figure 7 is significantly weakened after dividing the population by current SF activity. Instead, for the star-forming population, galaxy age is better correlated with $M_{*,FIT}$ (also seen in Figure 6). A straightforward interpretation is that when galaxies are growing rapidly through SF–that is, when they are located on or near the SF 'Main Sequence'–then M_* mostly traces how long this main SF phase has lasted

so far. In other words, M_* simply traces the build-up of the stellar population over time, while σ_* is related to the end of this main SF phase, i.e. to the regulation and cessation of SF, presumably through AGN feedback.

5.2. *Evolution of the average SFHs*

The average SFHs of galaxies, normalised by stellar mass, as a function of σ_* and $M_{*,FIT}$ are shown in Figure 8(a) and (b), respectively. The average SFHs were corrected for completeness by weighing each galaxy by a completeness correction factor to create a volume-limited quantity (see Wu et al. 2018). The population is divided by its current star-formation activity in order to disentangle the effects from these two populations as well as compare them. The velocity dispersion and mass ranges and were selected such that there were enough galaxies in each bin (≥ 10), in both quiescent and star-
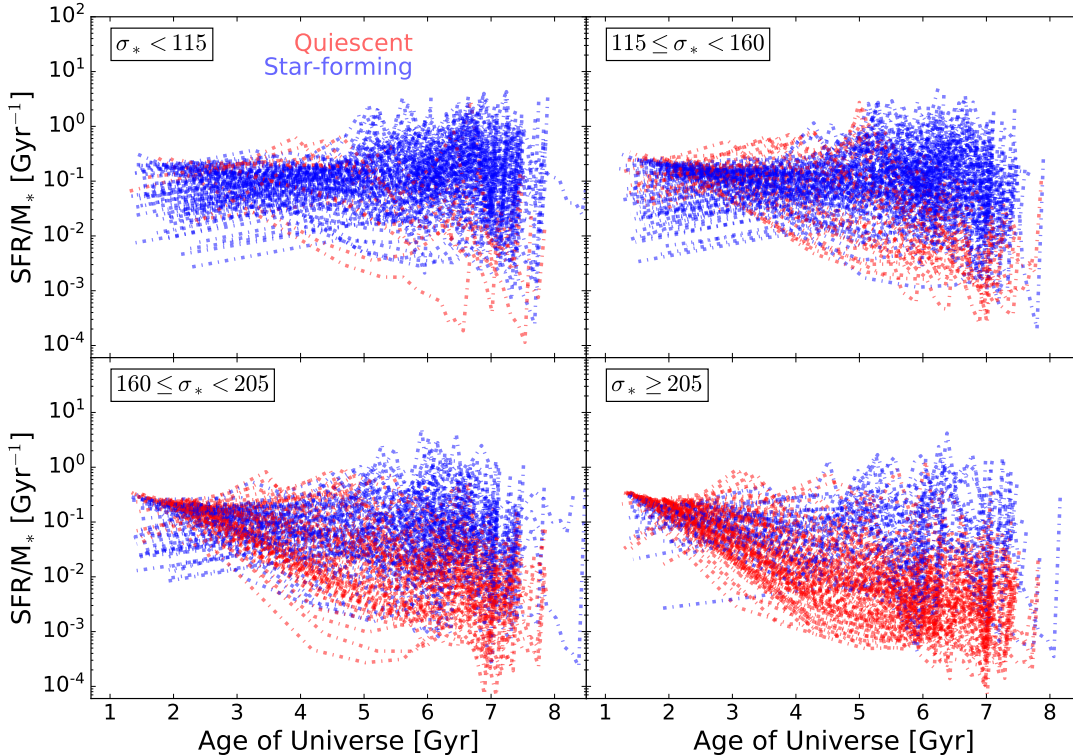
Figure 9. SFHs of the LEGA-C sample (normalised by stellar mass) as a function of the age of the Universe separated into four σ_* bins indicated by the labels. The colours differentiate between the star-forming and quiescent populations at the observed redshift.

forming galaxies. These relations are used to determine whether $z \sim 1$ galaxies also show a downsizing trend in their SFHs, as many studies have pointed to using local galaxies. However, the SFHs seen at $z \sim 1$ would not be resolved at $z \sim 0.1$, as the stellar populations would be too old.

On average, high-σ_* galaxies ($\sigma_* \geq 170\,\mathrm{km\,s^{-1}}$) had higher SFRs at earlier epochs which started to decline rapidly, at a rate that increases with σ_* and stellar mass, when the Universe was ~ 3 Gyrs old. Most galaxies with lower velocity dispersions ($\sigma_* < 170\,\mathrm{km\,s^{-1}}$) gradually build their stellar mass as the Universe evolves; however, the SFR of a minority, i.e. the quiescent population, began to decline when the Universe was ~ 5 Gyrs old. Higher-mass star-forming galaxies ($\mathrm{M_{*,FIT}} \geq 10^{10.5} M_\odot$) have SFHs that are consistent with constant star-formation with time, while the lower mass galaxies ($\mathrm{M_{*,FIT}} < 10^{10.5}$) still have rising SFRs. The star-forming population is still undergoing its main formation phase. The SFH trend is clear with $\mathrm{M_{*,FIT}}$ and not σ_* for the star-forming population, which extends from $\mathrm{M_{*,FIT}}$ being better correlated with SFHs for star-forming galaxies as discussed in Section 5.1 (see Figure 6 and 7).

Figure 8 reveals that, on average, most galaxies in the sample were forming stars quite early on; how-

ever, the SFRs were systematically higher and the eventual decline systematically more rapid with increasing σ_* ($\mathrm{M_{*,FIT}}$ for the star-forming population). This is clear evidence for the top-down scenario; where galaxies downsize in their star formation with time (more massive galaxies have older stars). This is seen in the overall population, and more strongly so in the quiescent population. While this result is in alignment with previous studies for the local universe (e.g. Juneau et al. 2005; Thomas et al. 2005; Tojeiro et al. 2009; McDermid et al. 2015; Ibarra-Medel et al. 2016), our work establishes this trend at $z \sim 1$ (half the current age of the Universe) using spectroscopy.

5.3. The variety of SFHs

In Figure 9, we show all the stellar mass normalised SFHs in the LEGA-C sample, separated into four velocity dispersion bins and divided into the quiescent and star-forming population (at the observed redshift) as defined in Section 5.1. This reveals the large scatter in the SFHs at fixed mass, in addition to discerning the differences in the histories based on the current star-formation activity of the galaxies.

The SFHs of quiescent galaxies peaked early on in the Universe and thereafter, their activity generally decreases with time; while star-forming galaxies gradually

grow in SFR, which peaked at later epochs. The quiescent population has consistently higher SFRs at early epochs, whereas its star-forming counterpart has higher SFRs at later epochs. This indicates that star-forming galaxies aggregate their mass slower than the quiescent population. The dominance of the quiescent population increases from low to high-mass galaxies, and vice versa for the star-forming population.

The SFRs of low mass galaxies ($\sigma_* < 115 \, \mathrm{km \, s^{-1}}$) have been gradually increasing, with large scatter at all epochs. These galaxies are currently undergoing the main stages of their star formation. Note that the lowest dispersion bin suffers from incompleteness, due to the survey sample selection approach. K-band quiescent galaxies are fainter than equally massive star-forming galaxies which causes an under-representation in the LEGA-C sample. However, it is well known that low-mass star-forming galaxies outnumber quiescent galaxies of the same mass; therefore, the SFHs in Figure 9 can be considered as illustrative.

The quiescent and star-forming populations are more evenly distributed (in number and variation of SFHs) in the intermediate-σ_* regime (between 160 and $205 \, \mathrm{km \, s^{-1}}$) while the high-$\sigma_*$ population ($\sigma_* \geq 205 \, \mathrm{km \, s^{-1}}$) is dominated by quiescent galaxies. The disparity between the SFHs of the quiescent and star-forming populations in the high-σ_* regime indicates that galaxies 'remember' their past. There is a strong coherence among the SFHs of quiescent and star-forming galaxies, respectively. This behaviour extends to the peak of cosmic SF activity at $z \sim 2$-3. This implies that SF activity at the moment of observation is strongly correlated with the SF activity $\sim 3 \, \mathrm{Gyrs}$ prior. The results of this work indicate that many evolutionary paths can lead to galaxies at a given velocity dispersion. This illustrates the difficulty of connecting progenitor and descendant populations at different cosmic epochs.

5.4. *Comparisons to Literature Measurements*

As stated in Section 5.2, the deconstructed SFHs in this study support the galaxy downsizing scenario which has long been studied (see Section 1). Leitner (2012)'s finding that star-forming galaxies formed only $\sim 15 \, \%$ of their mass before $z = 1$-2 (mass dependent), suggesting that present-day star-forming galaxies are not the descendants of massive star-forming galaxies at $z > 2$, is in line with our results since the peak in star formation occurs after $z < 1.5$ for almost all star-forming galaxies in the LEGA-C sample.

Intermediate-redshift stellar population studies are sparse, due to the high S/N required to undertake such studies (see Section 1). Pertaining to this work, there are a few studies we can draw comparisons from, viz. Choi et al. (2014) and Gallazzi et al. (2014). Measurements by Choi et al. (2014) and Gallazzi et al. (2014) indicating that passive galaxies have ages consistent with mostly passive evolution are also in alignment with this study as the reconstructed SFHs indicate that galaxies stay quiescent, barring some histories that showed low-level star formation after quiescence. Gallazzi et al. (2014) reported an average lighted-weighted age of $\sim 5 \, \mathrm{Gyrs}$ for a $4 \times 10^{10} \, \mathrm{M_\odot}$ galaxy, consistent with our value of $4.8 \, \mathrm{Gyrs}$, for a galaxy of the same mass.

Diemer et al. (2017) tested Gladders et al. (2013)'s hypothesis that the SFHs of individual galaxies are characterised by a log-normal function in time, which implies a slow decline in SFRs rather than rapid quenching. They did this by comparing the log-normal parameter space of total stellar mass, peak time, and full width at half maximum of simulated galaxies from Illustris (Vogelsberger et al. 2014) and Gladders et al. (2013), as well as Pacifici et al. (2016)'s derived SFHs of a sample of quiescent galaxies using a large library of computed theoretical SFHs. They found good agreement for all three studies, however, Illustris predicted more extended SFHs on average. LEGA-C galaxies support the slow-quenching picture of galaxy evolution as Gladders et al. (2013) have suggested, with a rate of decline that is mass dependent as we have seen. More comparisons will be performed in later papers.

6. SUMMARY

We have reconstructed the SFHs of galaxies in the current LEGA-C sample, which contains 678 primary sample galaxies with $\mathrm{S/N} \sim 20 \, \mathrm{\AA^{-1}}$ in the redshift range $0.6 < z < 1$. We have done this by implementing an algorithm to fit flexible SFHs to the full spectrum, using *FSPS* and *emcee*. The galaxy spectra were fit to a linear combination of a defined set of 12 CSPs, with solar metallicity and constant star formation within the time interval of the templates. In 90% of the cases the algorithm produced good fits based on the normalised χ^2 values. We found a wide variety of SFHs, although 60% of the galaxies have $\mathrm{a}_{<MW>} > 3 \, \mathrm{Gyrs}$ by the time we observe them (Figures 3 and 4). However, we note that age estimates from spectral fits experience increasing degeneracy of spectral features as the stellar populations age. Most of the old galaxies ($\mathrm{a}_{<MW>} \gtrsim 3 \, \mathrm{Gyrs}$) had very low SFRs early on ($\gtrsim 6 \, \mathrm{Gyrs}$ after the Big Bang, Figure 4). However, some exhibit subsequent peaks in star formation, which could be an indication of rejuvenated star formation, or a merger with a younger population. However, the mass formed from this more recent star formation activity is only about 10% of the mass

formed throughout the galaxies' histories. The median $a_{<LW>}$, $a_{<MW>}$ and $M_{*,FIT}$ were found to be 1.2 Gyrs, 3.8 Gyrs and $10^{10.8}$ M$_\odot$, respectively.

The main objective of this work was to investigate how our reconstructed SFHs behave as a function of stellar mass, stellar velocity dispersion and star-formation (SF) activity, as well as the variation they show at fixed velocity dispersion. We found that galaxies at $z \sim 1$ have similar trends in their SFHs compared to local galaxies, i.e. the stellar content in massive galaxies formed earlier and faster (Figure 8). This top-down scenario is a known trend from fossil record inferences using SDSS spectra; however, in this study, it is shown for $z \sim 1$ galaxies for the first time. We found that the scatter between the quiescent and star-forming populations increases towards lower redshift (Figure 9), which indicates that current SF activity is strongly correlated with past SF activity. High-dispersion quiescent galaxies had their star formation peak early, > 9.5 Gyrs ago, and exhibit decreasing SFRs throughout the rest of their history, for the most part. We found that the lowest dispersion galaxies in our sample are undergoing the main stage of their star formation as we observe them (7 Gyrs ago).

The results of the spectral fits were used to measure a number of galaxy properties, viz. ages ($a_{<LW>}$, $a_{<MW>}$, $a_{<MW>}$, etc.) and stellar mass, in order to test the model by investigating how these properties relate to one another as well as other properties measured from the galaxy spectra, e.g. velocity dispersion, $H\delta$, $D_n 4000$, etc. We showed that galaxies evolve from the top-left to the bottom-right of the EW(Hδ)-D$_n$4000 plane as they age, as would be expected (Figure 5).

Recovering the full SFHs of intermediate-redshift galaxies opens up a multitude of avenues of research. In this work we have shown the clear differences between the SFHs of quiescent and star-forming galaxies and how these SFHs are scattered at fixed velocity dispersion. We have also shown that velocity dispersion is a better indicator of the age and current SF activity of galaxies as a whole than stellar mass, while stellar mass is a better indicator of the age of star-forming galaxies (Figure 6 and 7). In future studies, we will use the reconstructed SFHs to constrain the quenching speed and rate, as well as investigate the relationship between galactic structure and SFHs. These constraints will become valuable for future surveys like JWST that will be investigating the properties of galaxies beyond $z \sim 2$, and will need $z \sim 1$ measurements as a benchmark to connect those populations to the local Universe.

7. ACKNOWLEDGEMENTS

REFERENCES

Abramson, L. E., Gladders, M. D., Dressler, A., et al. 2016, ApJ, 832, 7

Barišić, I., van der Wel, A., Bezanson, R., et al. 2017, ApJ, 847, 72

Barro, G., Faber, S. M., Koo, D. C., et al. 2017, ApJ, 840, 47

Belli, S., Newman, A. B., & Ellis, R. S. 2015, ApJ, 799, 206

Best, P. N., Kauffmann, G., Heckman, T. M., & Ivezić, Ž. 2005, MNRAS, 362, 9

Brammer, G. B., Whitaker, K. E., van Dokkum, P. G., et al. 2011, ApJ, 739, 24

Bruzual, G., & Charlot, S. 2003, MNRAS, 344, 1000

Calzetti, D., Armus, L., Bohlin, R. C., et al. 2000, ApJ, 533, 682

Cappellari, M., & Emsellem, E. 2004, PASP, 116, 138

Chabrier, G. 2003, PASP, 115, 763

Charlot, S., & Fall, S. M. 2000, ApJ, 539, 718

Choi, J., Conroy, C., Moustakas, J., et al. 2014, ApJ, 792, 95

Cid Fernandes, R., Asari, N. V., Sodré, L., et al. 2007, MNRAS, 375, L16

Cid Fernandes, R., Mateus, A., Sodré, L., Stasińska, G., & Gomes, J. M. 2005, MNRAS, 358, 363

Cimatti, A., Daddi, E., & Renzini, A. 2006, A&A, 453, L29

Conroy, C., & Gunn, J. E. 2010, ApJ, 712, 833

Conroy, C., Gunn, J. E., & White, M. 2009, ApJ, 699, 486

Diemer, B., Sparre, M., Abramson, L. E., & Torrey, P. 2017, ApJ, 839, 26

Foreman-Mackey, D., Hogg, D. W., Lang, D., & Goodman, J. 2013, PASP, 125, 306

Foreman-Mackey, D., Sick, J., & Johnson, B. 2014,
    doi:10.5281/zenodo.12157.
    https://doi.org/10.5281/zenodo.12157

Franx, M., van Dokkum, P. G., Förster Schreiber, N. M.,
    et al. 2008, ApJ, 688, 770

Gallazzi, A., Bell, E. F., Zibetti, S., Brinchmann, J., &
    Kelson, D. D. 2014, ApJ, 788, 72

Gallazzi, A., Charlot, S., Brinchmann, J., White, S. D. M.,
    & Tremonti, C. A. 2005, MNRAS, 362, 41

Girardi, L., Bressan, A., Bertelli, G., & Chiosi, C. 2000,
    A&AS, 141, 371

Gladders, M. D., Oemler, A., Dressler, A., et al. 2013, ApJ,
    770, 64

Goodman, J., & Weare, J. 2010, Communications in
    Applied Mathematics and Computational Science, Vol. 5,
    No. 1, p. 65-80, 2010, 5, 65

Graves, G. J., Faber, S. M., & Schiavon, R. P. 2009, ApJ,
    698, 1590

Heavens, A. F., Jimenez, R., & Lahav, O. 2000, MNRAS,
    317, 965

Ibarra-Medel, H. J., Sánchez, S. F., Avila-Reese, V., et al.
    2016, MNRAS, 463, 2799

Jørgensen, I., & Chiboucas, K. 2013, AJ, 145, 77

Jørgensen, I., Chiboucas, K., Berkson, E., et al. 2017, AJ,
    154, 251

Juneau, S., Glazebrook, K., Crampton, D., et al. 2005,
    ApJL, 619, L135

Karim, A., Schinnerer, E., Martínez-Sansigre, A., et al.
    2011, ApJ, 730, 61

Kauffmann, G., Heckman, T. M., White, S. D. M., et al.
    2003, MNRAS, 341, 54

Khostovan, A. A., Sobral, D., Mobasher, B., et al. 2015,
    MNRAS, 452, 3948

Koleva, M., Prugniel, P., Bouchard, A., & Wu, Y. 2009,
    A&A, 501, 1269

Kriek, M., van Dokkum, P. G., Labbé, I., et al. 2009, ApJ,
    700, 221

Kriek, M., Conroy, C., van Dokkum, P. G., et al. 2016,
    Nature, 540, 248

Kroupa, P., Aarseth, S., & Hurley, J. 2001, MNRAS, 321,
    699

Leitner, S. N. 2012, ApJ, 745, 149

Madau, P., & Dickinson, M. 2014, ARA&A, 52, 415

Maraston, C., Strömbäck, G., Thomas, D., Wake, D. A., &
    Nichol, R. C. 2009, MNRAS, 394, L107

Marigo, P., & Girardi, L. 2007, A&A, 469, 239

Marigo, P., Girardi, L., Bressan, A., et al. 2008, A&A, 482,
    883

McDermid, R. M., Alatalo, K., Blitz, L., et al. 2015,
    MNRAS, 448, 3484

Mosleh, M., Tacchella, S., Renzini, A., et al. 2017, ApJ,
    837, 2

Moustakas, J., Coil, A. L., Aird, J., et al. 2013, ApJ, 767, 50

Muzzin, A., Marchesini, D., Stefanon, M., et al. 2013a,
    ApJ, 777, 18

—. 2013b, ApJS, 206, 8

Ocvirk, P., Pichon, C., Lançon, A., & Thiébaut, E. 2006,
    MNRAS, 365, 46

Onodera, M., Carollo, C. M., Renzini, A., et al. 2015, ApJ,
    808, 161

Pacifici, C., Kassin, S. A., Weiner, B. J., et al. 2016, ApJ,
    832, 79

Pozzetti, L., Bolzonella, M., Zucca, E., et al. 2010, A&A,
    523, A13

Sánchez-Blázquez, P., Peletier, R. F., Jiménez-Vicente, J.,
    et al. 2006, MNRAS, 371, 703

Terrazas, B. A., Bell, E. F., Henriques, B. M. B., et al.
    2016, ApJL, 830, L12

Thomas, D., Maraston, C., Bender, R., & Mendes de
    Oliveira, C. 2005, ApJ, 621, 673

Thomas, D., Maraston, C., Schawinski, K., Sarzi, M., &
    Silk, J. 2010, MNRAS, 404, 1775

Toft, S., Gallazzi, A., Zirm, A., et al. 2012, ApJ, 754, 3

Tojeiro, R., Heavens, A. F., Jimenez, R., & Panter, B.
    2007, MNRAS, 381, 1252

Tojeiro, R., Wilkins, S., Heavens, A. F., Panter, B., &
    Jimenez, R. 2009, ApJS, 185, 1

Torrey, P., Wellons, S., Ma, C.-P., Hopkins, P. F., &
    Vogelsberger, M. 2017, MNRAS, 467, 4872

van de Sande, J., Kriek, M., Franx, M., et al. 2013, ApJ,
    771, 85

van der Wel, A., Bell, E. F., van den Bosch, F. C., Gallazzi,
    A., & Rix, H.-W. 2009, ApJ, 698, 1232

van der Wel, A., Noeske, K., Bezanson, R., et al. 2016,
    ApJS, 223, 29

van Dokkum, P. G., & Brammer, G. 2010, ApJL, 718, L73

Vogelsberger, M., Genel, S., Springel, V., et al. 2014,
    MNRAS, 444, 1518

Weisz, D. R., Dalcanton, J. J., Williams, B. F., et al. 2011,
    ApJ, 739, 5

Whitaker, K. E., van Dokkum, P. G., Brammer, G., &
    Franx, M. 2012, ApJL, 754, L29

Whitaker, K. E., van Dokkum, P. G., Brammer, G., et al.
    2013, ApJL, 770, L39

Wilkinson, D. M., Maraston, C., Thomas, D., et al. 2015,
    MNRAS, 449, 328

Wu, P.-F., van der Wel, A., Gallazzi, A., et al. 2018, ArXiv
    e-prints, arXiv:1802.06799

York, D. G., Adelman, J., Anderson, Jr., J. E., et al. 2000,
    AJ, 120, 1579